nature medicine

In vivo imaging of inflammasome activation reveals a subcapsular macrophage burst response that mobilizes innate and adaptive immunity

Pervinder Sagoo[1,2], Zacarias Garcia[1,2], Beatrice Breart[1,2], Fabrice Lemaître[1,2], David Michonneau[1,2], Matthew L Albert[3,4], Yves Levy[5–8] & Philippe Bousso[1,2,5]

The inflammasome is activated in response to a variety of pathogens and has an important role in shaping adaptive immunity, yet the spatiotemporal orchestration of inflammasome activation *in vivo* and the mechanisms by which it promotes an effective immune response are not fully understood. Using an *in vivo* reporter to visualize inflammasome assembly, we establish the distribution, kinetics and propagation of the inflammasome response to a local viral infection. We show that modified vaccinia Ankara virus induces inflammasome activation in subcapsular sinus (SCS) macrophages, which is immediately followed by cell death and release of extracellular ASC specks. This transient inflammasome signaling in the lymph node generates a robust influx of inflammatory cells and mobilizes T cells from the circulation to increase the magnitude of T cell responses. We propose that after infection, SCS macrophages deliver a burst response of inflammasome activity and cell death that translates into the broadening of T cell responses, identifying an important aspect of inflammasome-driven vaccination strategies.

Innate immune sensing of pathogens or damage is characterized by activation of membrane and cytosolic pattern-recognition receptors including Toll-like receptors (TLRs), retinoic acid inducible gene I–like helicase receptors, cytosolic DNA sensors and NOD-like receptors[1]. The inflammasome forms part of this first-line response, mediated primarily by phagocytic antigen-presenting cells such as macrophages and dendritic cells, and refers to a hetero-multimeric protein scaffold assembled upon activation of cytosolic pattern-recognition receptors[2]. Multiple inflammasome complexes exist, each triggered by several cytosolic sensor families with specificities for distinct pattern-recognition motifs[2]. Once activated, many of these sensors associate with apoptosis-associated speck-like protein with a CARD domain (ASC), a common adaptor protein that promotes recruitment and proximity-induced autocatalytic maturation of caspase-1 (ref. 3). These processes occur through prion-like polymerization of ASC into filaments and ultimately result in the formation of micrometer-sized structures referred to as ASC specks[4].

Inflammatory effector mechanisms unleashed by active caspase-1 include the proteolytic processing and release of interleukin-1β (IL-1β) and IL-18 and induction of cellular pyroptotic death[4,5]. *In vitro*, ASC speck formation can coincide with cell death and cytokine release[6,7], but the relationship between inflammasome activation *in vivo* and induction of cell death remains to be documented. Recent studies have provided evidence that ASC specks can exist as active extracellular structures, raising interest in the fate and dynamics of ASC specks after cell death[8,9]. Despite an increasing knowledge of effector mechanisms induced by the inflammasome response, understanding of how inflammasome activation unfolds *in vivo* is still limited. In particular, the location and timing of inflammasome activity in tissue is unclear, as are the immediate effects of cellular inflammasome activity. Although several fluorescent probes have been developed to study inflammasome activation *in vitro*[10–12], their use for *in vivo* applications has remained challenging, lacking translation to single-cell resolution at the organ level[10,12,13].

Another question in inflammasome biology is how its activity regulates innate and adaptive immunity. Proinflammatory IL-1 and IL-18 have been shown to have roles in local and peripheral recruitment and priming of the immune response[14–17], and the absence of inflammasome activity has been associated with poor pathogen clearance and increased disease severity[17–21]. Mechanisms that link the inflammasome pathway to T cell responses include danger-associated molecular pattern (DAMP)-mediated dendritic cell (DC) activation[22], effects of inflammatory cytokines on T cell polarization[23] and activation or noncognate induction of interferon-γ (IFN-γ) in memory T cells[16,24]. In this respect, understanding the spatiotemporal dynamics of inflammasome activation may help clarify the downstream effects on the T cell response. Here we establish an *in vivo* reporter system to visualize inflammasome activation in real time and dissect its influence on the immune response after local viral infection.

[1]Dynamics of Immune Responses Unit, Institut Pasteur, Paris, France. [2]Institut National de la Santé et de la Recherche Médicale U668, Paris, France. [3]Laboratory of Dendritic Cells Immunobiology, Institut Pasteur, Paris, France. [4]Institut National de la Santé et de la Recherche Médicale U818, Paris, France. [5]Vaccine Research Institute, Créteil, France. [6]Institut National de la Santé et de la Recherche Médicale U955, Créteil, France. [7]Faculté de Médecine, Université Paris Est, Créteil, France. [8]Service d'Immunologie Clinique et Maladies Infectieuses, Hôpital H. Mondor-A. Chenevier, Créteil, France. Correspondence should be addressed to P.B. (philippe.bousso@pasteur.fr).

Received 9 October; accepted 20 November; published online 21 December 2015; doi:10.1038/nm.4016

RESULTS

MVA induces inflammasome activation in macrophages

To examine local viral infection as an inflammasome trigger, we selected MVA, a replication-deficient group I double-stranded DNA poxvirus used in clinical vaccination programs, with strong immunogenicity through activation of endosomal TLRs and cytosolic melanoma differentiation-associated protein 5 (MDA-5), Absent in melanoma 2 (AIM2) and NOD-like receptor NLRP3 (refs. 25–27). As such, it delivers a temporally defined stimulus for inflammasome activation, allowing a model for direct monitoring of downstream cellular events of infection. Using both wild-type (WT) and caspase-1–deficient (*Casp1*$^{-/-}$; *Casp4*$^{-/-}$) mouse strains, we confirmed that MVA infection induced inflammasome activity in bone marrow–derived macrophages (BMDMs) by detection of caspase-1 activity (**Fig. 1a** and **Supplementary Fig. 1a**) and IL-1β (**Fig. 1b**). Addition of the caspase-1–specific inhibitor Z-YVAD-FMK prevented IL-1β release induced by ATP treatment of lipopolysaccharide (LPS)-primed BMDMs or MVA-infected BMDMs, demonstrating that IL-1β release depends on the conventional inflammasome pathway[28,29].

To detect inflammasome activation in real time, we stably transduced BMDMs to express a fusion protein of ASC and GFP (ASC-GFP) as a read-out for inflammasome assembly. As anticipated, MVA infection induced formation of ASC specks *in vitro* (**Fig. 1c**,**d**), which could be visualized by redistribution of ASC-GFP as it oligomerizes to form a single macromolecular complex[30] (**Supplementary Movie 1**). Concomitant with inflammasome activity, MVA infection also induced caspase-1–dependent macrophage death (**Fig. 1e**). *In vitro*, ASC-GFP expression in BMDMs did not alter cellular levels of caspase-1 activity, IL-1β release or the kinetics or amount of cell death (**Supplementary Fig. 1b**–**f**). These observations correspond with a recent report highlighting the crucial role of the levels of upstream inflammasome sensor proteins in determining the rate of speck formation[4]. *In vivo*, after local viral infection (subcutaneous footpad injection) with MVA, we found that virus primarily targeted macrophages within the subcapsular (SCS-M) and medullary regions of the draining lymph node, consistent with previous reports of their role in sequestering lymph-borne pathogens[31–33] (**Supplementary Fig. 2**). MVA infection resulted in rapid and specific loss of lymph node macrophages, most notably CD169^{+}F4/80^{-} SCS-Ms (**Fig. 1f**,**g**). These findings suggest that inflammasome signaling and pyroptotic death may be an important component of the immune response to MVA.

SCS macrophages initiate the inflammasome response to MVA

Detection of inflammasome activity *in vivo* at single-cell resolution has so far been restricted to static imaging on fixed tissue sections[34], limiting an understanding of the identity, dynamics and fate of cells undergoing inflammasome activation. This is due to the lack of mouse models to detect inflammasome activation and in part to the inherently transient nature of cell signaling that may ultimately progress to cellular demise.

To circumvent this limitation, we developed a strategy for dynamic two-photon imaging of inflammasome assembly by *in vivo* detection of ASC speck formation. Mixed bone marrow–chimeric (BM chimeric) mice were generated by transfer of cycling bone marrow–derived hematopoietic stem cells (BM-HSCs) retrovirally transduced to express ASC-GFP. ASC-GFP-expressing BM-HSCs derived from *Rag2*$^{-/-}$ mice were mixed with either WT or caspase-1–deficient BM-HSCs and used to reconstitute recipient mice (**Fig. 2a**). This strategy served to restrict reporter expression to the myeloid compartment and limit caspase-1–dependent functional inflammasome signaling to cells expressing the reporter. Within lymph nodes of chimeric mice, ASC-GFP was expressed by myeloid cells, with a normal distribution throughout the lymph node volume (**Supplementary Fig. 3a**,**b**). Intravital imaging of chimeric mice revealed ASC-GFP expression by cells localized to the subcapsular sinus region of resting lymph nodes (**Fig. 2b**). These cells formed a dense network at the lymph node periphery, displayed a macrophage-like morphology and were stained after *in vivo* injection of a CD169-specific antibody (**Fig. 2c**), indicating myeloid-derived reconstitution of lymph node subcapsular sinus macrophages, as previously described[35].

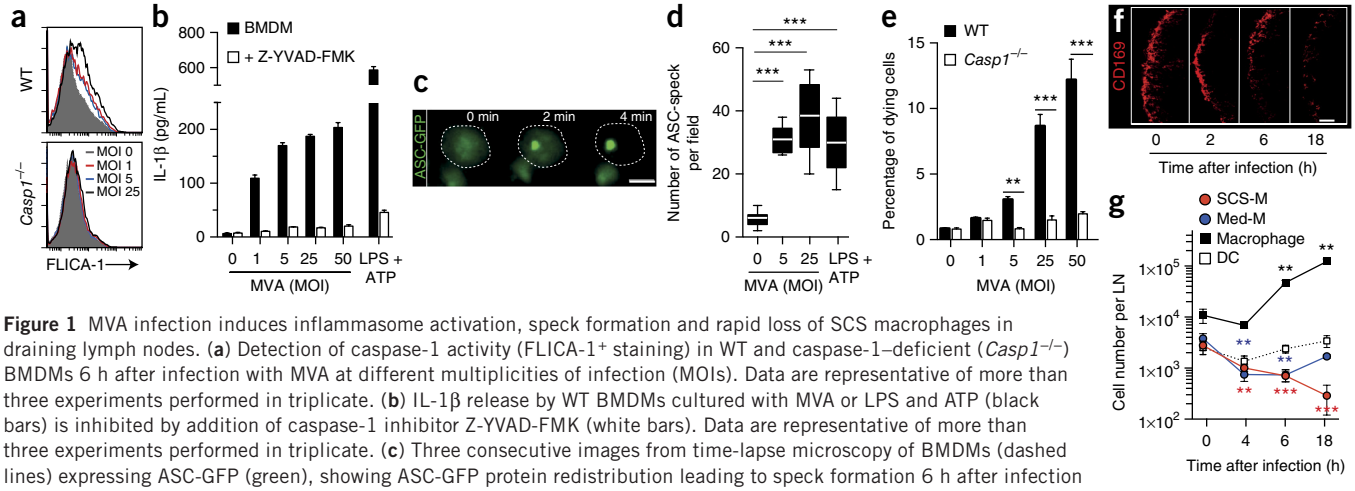

Figure 1 MVA infection induces inflammasome activation, speck formation and rapid loss of SCS macrophages in draining lymph nodes. (**a**) Detection of caspase-1 activity (FLICA-1^{+} staining) in WT and caspase-1–deficient (*Casp1*$^{-/-}$) BMDMs 6 h after infection with MVA at different multiplicities of infection (MOIs). Data are representative of more than three experiments performed in triplicate. (**b**) IL-1β release by WT BMDMs cultured with MVA or LPS and ATP (black bars) is inhibited by addition of caspase-1 inhibitor Z-YVAD-FMK (white bars). Data are representative of more than three experiments performed in triplicate. (**c**) Three consecutive images from time-lapse microscopy of BMDMs (dashed lines) expressing ASC-GFP (green), showing ASC-GFP protein redistribution leading to speck formation 6 h after infection with MVA (MOI = 25). Scale bar, 10 μm. Representative images from more than 10 independent experiments. (**d**) Detection of ASC specks in cultures of WT BMDMs expressing ASC-GFP, 15 h after treatment with MVA or LPS + ATP. (**e**) Percentage of dying cells (assessed by flow cytometry for propidium iodide staining) in WT and *Casp1*$^{-/-}$ BMDM cultures 6 h after MVA infection. Data are representative of more than three experiments performed in triplicate. (**f**) Immunofluorescence staining of CD169^{+} antigen in popliteal lymph nodes from WT mice up to 18 h after subcutaneous injection of MVA (5×10^{6} plaque-forming units (p.f.u.)) showing loss of SCS-macrophages (SCS-Ms) from subcapsular sinus regions of lymph nodes. Scale bar, 100 μm. Representative of four experiments, $n = 3$ mice per group. (**g**) Flow cytometry detection of numbers of lymph node SCS-M, medullary macrophage (med-M), macrophage and dendritic cell (DC) subsets in WT mice after injection of MVA. Representative of more than 6 experiments, $n = 6$ mice per time point. Error bars, mean ± s.e.m. $^{**}P < 0.01$, $^{***}P < 0.001$, one-way analysis of variance (ANOVA) followed by Tukey's *post hoc* test for multiple comparison (**d**) or Student's *t*-test (**e**,**g**).

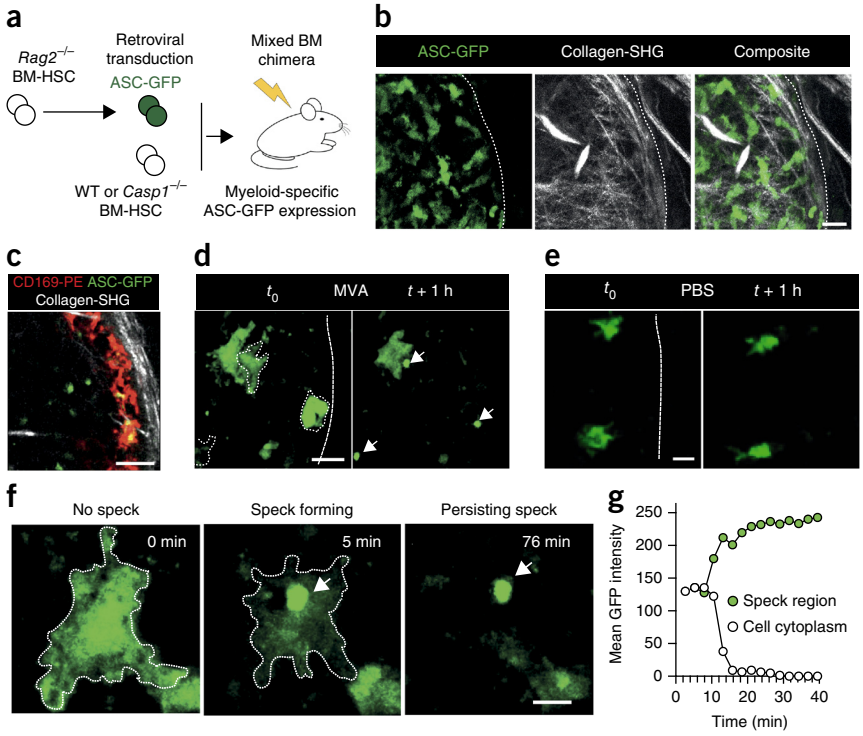

Figure 2 Dynamic imaging of inflammasome activation in ASC-GFP retrogenic mice reveals rapid kinetics of cellular inflammasome signaling. (**a**) Chimeras generated by transfer of *Rag2*$^{-/-}$ BM-HSCs transduced to express ASC-GFP into irradiated recipient mice with WT or *Casp1*$^{-/-}$ BM cells. (**b**) Intravital microscopy of the popliteal lymph node in ASC-GFP BM chimeras, showing GFP (green) expression in cells localized to the lymph node collagen capsule (white). Dashed lines indicate lymph node edge. Scale bar, 30 µm. SHG, second harmonics generation. (**c**) Intravital view of ASC-GFP BM chimeric mouse lymph node after *in vivo* staining with phycoerythrin (PE)-conjugated anti-CD169 showing GFP^{+} cell and CD169 colocalization in the subcapsular sinus region. Scale bar, 30 µm. (**d**,**e**) Intravital images of ASC-GFP BM chimeric mouse lymph node over a time (*t*) interval of 1 h after injection with MVA (**d**) or PBS (**e**). Arrows indicate ASC speck formation events; dashed lines indicate lymph node edge and delineate individual ASC-GFP expressing cells. Scale bars, 30 µm. (**f**) Intravital images of ASC speck formation in a lymph node macrophage 3 h after local infection with MVA. *t* is relative to start of ASC-GFP redistribution during speck formation. Scale bar, 10 µm. (**g**) Kinetics of speck formation *in vivo* detected by redistribution of ASC-GFP protein (change in mean GFP intensity) from cell cytoplasm to the speck region in a single lymph node macrophage on local MVA infection. Data are representative of 36 individual mice (**b**–**f**) or representative of more than 40 independent events (**g**).

When ASC-GFP chimeric mice were injected subcutaneously with MVA, we detected ASC speck formation primarily within these macrophages in draining lymph nodes (**Fig. 2d** and **Supplementary Movie 2**). Of note, we did not observe ASC speck formation in chimeric mice injected with PBS (**Fig. 2e** and **Supplementary Movie 3**). Single-cell analysis of the redistribution of ASC-GFP leading to speck assembly revealed a rapid and dynamic cellular process (**Fig. 2f**,**g**), with the majority of cells undergoing complete ASC oligomerization within 10 min (mode, 2.8 min; median, 6 min; range, 2–99 min) (**Fig. 3a** and **Supplementary Fig. 3c**).

We next quantified ASC speck formation occurring during the first 12 h after local MVA injection and identified an acute inflammasome response, detectable within 1 h after infection and peaking over the subsequent 2 h (**Fig. 3b**). For these analyses we counted ASC specks that formed during imaging (referred to as forming ASC specks) and ASC specks that had already formed (referred to as formed ASC specks) at the time of imaging. Inflammasome activation then steadily declined until neither forming nor formed specks were detected at 12 h. The number of ASC specks detected after infection corresponded with the kinetics of SCS-M loss observed by histological and lymph node cell-suspension analysis methods described above (**Fig. 1f**,**g**). Thus the steady decline in the numbers of specks detected after infection probably reflects the loss of SCS-Ms. Throughout the imaging period, ASC specks were not detected in lymph nodes of PBS-injected controls or within deeper regions of the lymph node accessible by two-photon imaging after MVA injection (**Supplementary Movie 4**). Further analysis of the relative spatial arrangement of specks in the lymph node revealed that the majority were localized to within 30 µm of the subcapsular region, as indicated by the presence of capsular collagen fibers (**Fig. 3c** and **Supplementary Fig. 3d**,**e**). When compiled, these data reveal a rapid triggering of ASC speck formation, generating a transient and spatially confined wave of inflammasome activity spanning the first 7 h after infection.

Cell death and release of extracellular ASC specks *in vivo*

Pyroptosis is a caspase-1–dependent form of cell death[36] that, unlike other modes of cell death, is an inflammatory event associated with cell swelling, membrane lysis and nuclear condensation[37]. Using time-lapse microscopy, we examined infection (MVA-GFP), inflammasome activation (ASC-mCherry) and cell death (DNA-binding SytoxBlue) events in BMDMs in parallel (**Fig. 4a** and **Supplementary Movie 5**). Dynamic analysis of virally encoded GFP and nuclear stain intensities revealed that ASC speck formation in BMDMs was closely followed by loss of cell integrity and cellular demise (**Fig. 4b**). This process occurred within minutes after inflammasome assembly (mode, 3 min; median, 7 min; range, 0–40 min) and was largely intrinsic to cell infection, with no appreciable cell-to-cell transactivation of the inflammasome response to infection (**Supplementary Fig. 4a**,**b**). We next examined the process of ASC speck formation and cell death by *in vivo* labeling of lymph nodes with the cell-permeable nuclear DNA–binding dye Hoechst 33342 (Hoechst), enabling detection of cell-death events by tracking nuclear condensation. Intravital imaging revealed that macrophages undergoing inflammasome activation died rapidly after speck formation, progressing first to nuclear condensation and then to disappearance of the nucleus (**Fig. 4c** and **Supplementary Fig. 4c**).

While examining *in vivo* Hoechst labeling of draining lymph nodes, we noted that the majority of formed specks we detected did not have any associated nuclei, suggesting they were remnants of cells after inflammasome activation. To more firmly establish this hypothesis, we injected a fluorescence-conjugated antibody to ASC into MVA-infected ASC-GFP chimeric mice. Formed specks were counterstained

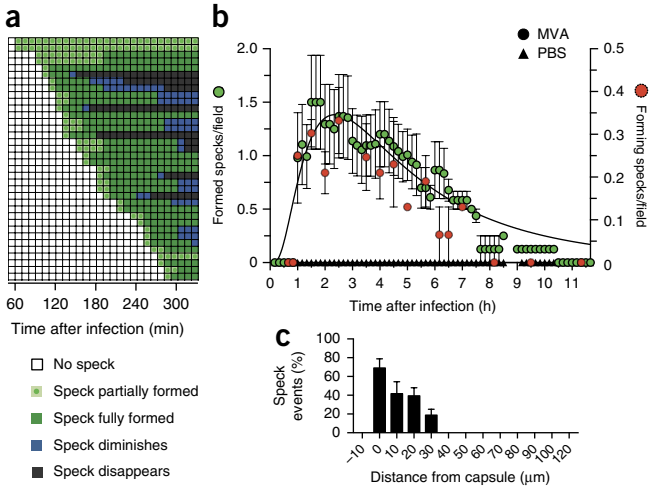

Figure 3 Subcapsular macrophages provide a spatiotemporally defined inflammasome response to local viral infection. (**a**) Intravital tracking of ASC speck formation and its kinetics in the popliteal lymph node after local MVA infection. Each row represents an individual ASC-GFP$^+$ cell; each square represents a 10-min period. Data are compiled from more than 40 independent events. (**b**) Quantification of inflammasome activity in draining lymph node 0–12 h after local injection of PBS or MVA. Numbers of formed and actively forming ASC specks detected by intravital microscopy per imaging field are shown. Each dot represents the mean ± s.e.m. number of events detected at each experimental time point (n = 8–33 movies acquired from at least three mice for each time point). Data are fit to a log Gaussian curve. (**c**) Percentage of ASC-GFP specks detected at distances up to 100 μm from the lymph node capsule; 0 μm was identified by second harmonics signal generation by collagen fibers. Data are mean ± s.e.m. of 35 speck events detected within 11 imaging fields (5 independent experiments), each acquired at imaging depths up to 100 μm.

with the ASC antibody, confirming their extracellular nature (**Fig. 4d**). Intravital tracking of formed specks over several hours revealed that many specks are long-lived entities, persisting for more than 4 h in the lymph node microenvironment (**Fig. 4e**). Moreover, specks generated *in vivo* remained as long-lasting structures, gradually diminished in size before eventually disappearing, suddenly disappeared or were fragmented into multiple specks (**Fig. 4e**,**f** and **Supplementary Movie 6**). In addition, on several occasions we observed the acquisition of specks by other cells within the lymph node (**Supplementary Movie 7**). These *in vivo* observations are consistent with two recent reports describing the ability of macrophages to phagocytize specks *in vitro*, with the potential to precipitate inflammasome activation within the engulfing cell[8,9].

In vivo analysis of inflammasome activity also revealed a phenomenon whereby ASC speck formation and subsequent cell death resulted in a rapid localized recruitment and clustering of resident cells toward newly generated specks (**Fig. 4g** and **Supplementary Movie 8**). Such recruitment occurred within minutes after speck formation and cell death and could be detected by Hoechst staining and by tracking myeloid cells (GFP$^+$) in ASC-GFP chimeras (**Supplementary Movie 8**). In summary, our results describe the rapid and localized initiation of inflammasome activation in the lymph node on viral infection, resulting in macrophage death, persistence of extracellular ASC specks and local cell recruitment.

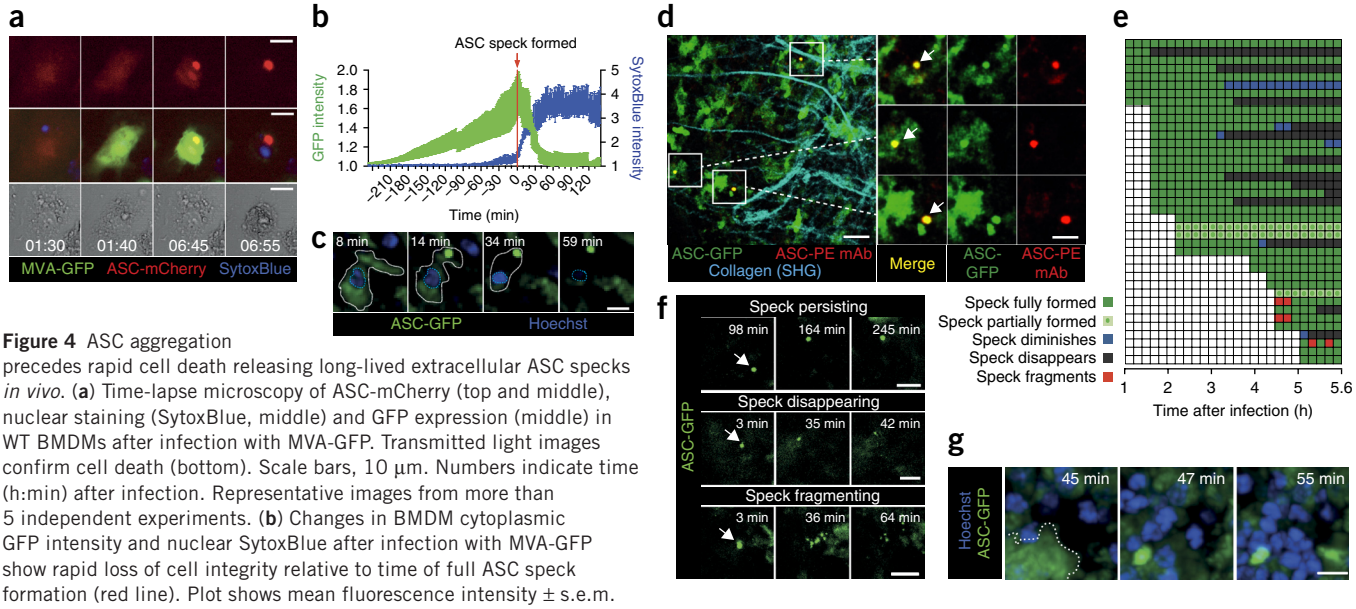

Figure 4 ASC aggregation precedes rapid cell death releasing long-lived extracellular ASC specks *in vivo*. (**a**) Time-lapse microscopy of ASC-mCherry (top and middle), nuclear staining (SytoxBlue, middle) and GFP expression (middle) in WT BMDMs after infection with MVA-GFP. Transmitted light images confirm cell death (bottom). Scale bars, 10 μm. Numbers indicate time (h:min) after infection. Representative images from more than 5 independent experiments. (**b**) Changes in BMDM cytoplasmic GFP intensity and nuclear SytoxBlue after infection with MVA-GFP show rapid loss of cell integrity relative to time of full ASC speck formation (red line). Plot shows mean fluorescence intensity ± s.e.m. for 25 cellular events. (**c**) *In situ* nuclear (Hoechst) staining of lymph node macrophages from ASC-GFP BM chimeric mice shows MVA-induced ASC speck formation is associated with rapid nuclear condensation. Scale bar, 10 μm. Dashed white lines indicate detectable cell cytoplasm; dashed blue lines indicate nuclear regions. Time points are from start of imaging. Images are representative of five independent experiments. (**d**) Intravital imaging of lymph nodes from ASC-GFP BM chimeric mice after MVA treatment (6 h) showing colocalization (arrows) of locally injected ASC-specific PE monoclonal antibody (mAb) with formed ASC-GFP specks. Scale bars, 40 μm (left) or 20 μm (inset). SHG, second harmonics generation. Images are representative of three independent experiments. (**e**) Intravital tracking of formed ASC specks induced by MVA infection. Rows represent individual formed specks tracked *in vivo*; each square shows changes observed over 10 min. Images representative of more than 80 independent events (n = 28 mice). (**f**) Intravital images of speck fates. Scale bars, 10 μm. Images representative of more than 80 independent events (n = 28 mice). Time points are from start of imaging. (**g**) *In situ* nuclear staining (Hoechst) of lymph node–resident cells and intravital imaging of ASC speck formation (green) in lymph nodes of ASC-GFP BM chimeric mice after MVA infection. Time points are from start of imaging. Scale bar, 10 μm. Images are representative of five independent experiments.

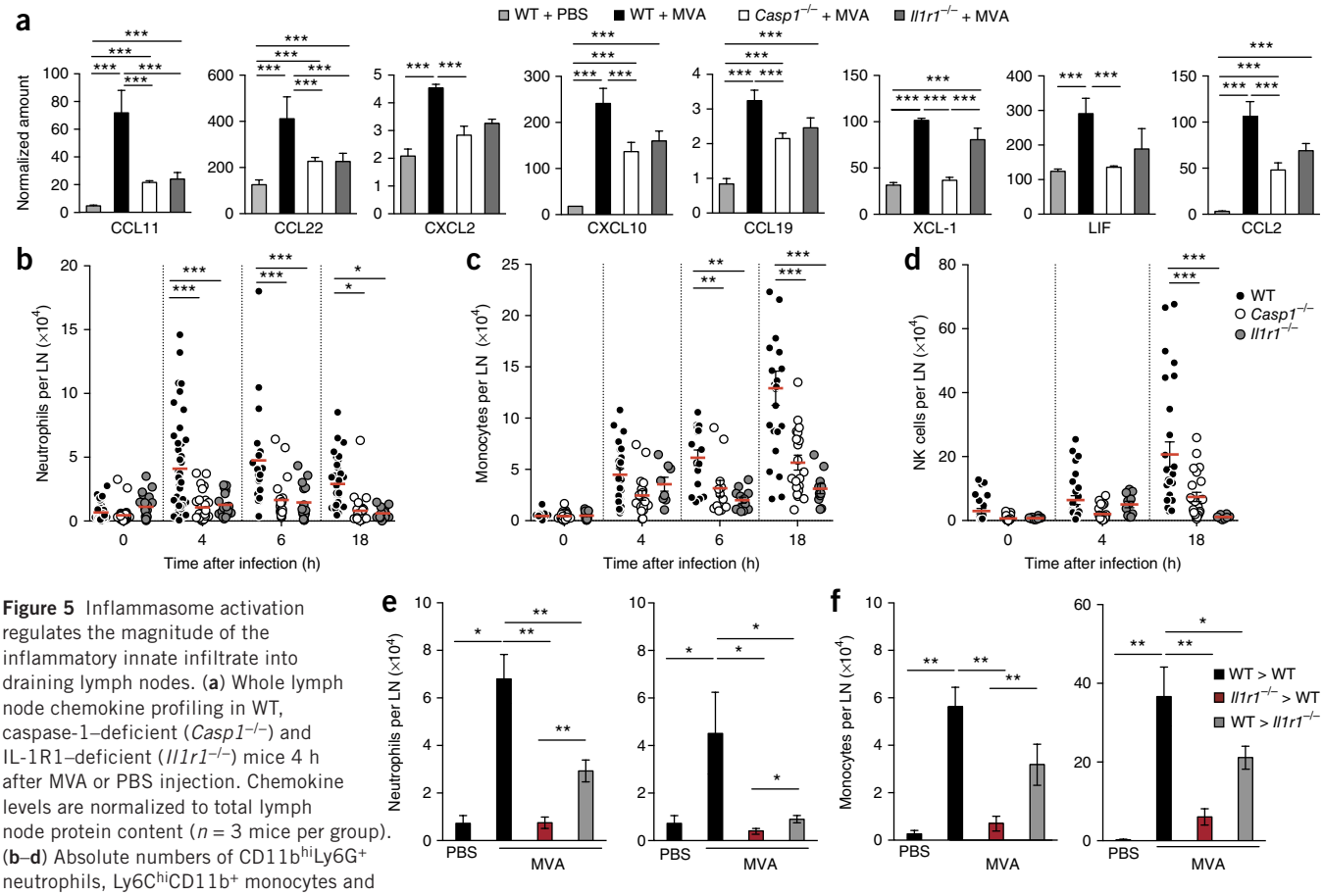

Figure 5 Inflammasome activation regulates the magnitude of the inflammatory innate infiltrate into draining lymph nodes. (**a**) Whole lymph node chemokine profiling in WT, caspase-1–deficient (*Casp1*$^{-/-}$) and IL-1R1–deficient (*Il1r1*$^{-/-}$) mice 4 h after MVA or PBS injection. Chemokine levels are normalized to total lymph node protein content ($n = 3$ mice per group). (**b**–**d**) Absolute numbers of CD11b^{hi}Ly6G^{+} neutrophils, Ly6C^{hi}CD11b^{+} monocytes and NK cells in lymph nodes as assessed by flow cytometry at various time points after subcutaneous MVA infection in WT (black circles), *Casp1*$^{-/-}$ (open circles) and *Il1r1*$^{-/-}$ (gray circles) mice. Data are combined from more than 6 independent experiments. (**e**,**f**) Absolute numbers of neutrophils (**e**) and monocytes (**f**) in lymph nodes of BM chimeric mice (*Il1r1*$^{-/-}$ > WT, red; WT > *Il1r1*$^{-/-}$, gray; control group WT > WT, black bars) as assessed by flow cytometry, 4 h (left) or 18 h (right) after MVA infection or control (PBS) injection. Data are representative of two independent experiments with $n = 5$ mice per group. Error bars, mean ± s.e.m. $^{*}P < 0.05$, $^{**}P < 0.01$, $^{***}P < 0.001$, one-way ANOVA with Tukey's multiple comparison test (**b**–**f**) or Mann-Whitney *U*-test (**a**). LN, lymph node.

Inflammasome signaling leads to influx of inflammatory cells

Our *in vivo* analysis revealed that inflammasome activation induced by MVA was restricted to the lymph node. Therefore, we next assessed how inflammasome signaling translates to activation of the innate and adaptive immune response by performing whole lymph node screening of chemokine mediators expressed early (4 h) after local viral infection (**Fig. 5a**). We observed rapid production of chemokines induced by MVA, many of which were reduced in the absence of caspase-1 or IL-1 receptor type 1 (IL-1R1) signaling (CCL11, CCL22, CXCL2, CXCL10 and CCL19). This shows that a transient wave of inflammasome activation elicited by MVA is a potent modulator of chemokine release in draining lymph nodes. Consistent with these data and previous reports on chemokine induction by MVA[25,38], this wave of chemokine release was associated with rapid and robust infiltration of neutrophils, monocytes and natural killer (NK) cells to the lymph node. Innate immune cell recruitment was substantially reduced in the absence of caspase-1 or IL-1R1 signaling (**Fig. 5b**–**d** and **Supplementary Fig. 5**).

To identify which cellular compartment was responsible for responding to inflammasome-derived IL-1 signals, we generated BM chimeric mice in which only hematopoietic cells (WT BM > *Il1r1*$^{-/-}$) or only nonhematopoietically derived cells (*Il1r1*$^{-/-}$ BM > WT) expressed IL-1R1. Infection-induced recruitment of neutrophils and monocytes was abolished in the absence of hematopoietic cellular sensing of IL-1 and was partially diminished by nonhematopoietic cell expression of IL-1R (**Fig. 5e**,**f**). This indicates that cells of predominantly hematopoietic origin relay IL-1 signals in the lymph node to promote infiltration of innate cells to the draining lymph node.

Inflammasome signals broaden composition of T cell responses

To assess the contribution of inflammasome activation to the adaptive immune response, we focused on the generation of the antigen-specific CD8^{+} T cell response directed against the immunodominant vaccinia viral peptide (VVp) B8R 20–27 expressed by MVA (**Fig. 6a**). Lack of caspase-1 activity or IL-1R1 expression resulted in moderately lower percentages of antigen-specific T cells induced by MVA infection (**Fig. 6b**). However, both caspase-1 and IL-1R1–deficient mice showed reduced absolute numbers of VVp-specific cells (**Fig. 6c**).

We hypothesized that an overall increase in leukocyte infiltration induced by inflammasome activity may lead to more naive T cells being recruited to the draining lymph node for priming and activation. Indeed, functional inflammasome and IL-1R1 signaling promoted the overall accumulation of CD8^{+} T cells in the draining lymph node as early as 18 h after MVA injection (**Fig. 6d**,**e**). To test whether inflammasome activation favors the recruitment of T cells that were not initially present in the lymph node, we transferred T cells into WT and caspase-1– and IL-1R1–deficient recipients and

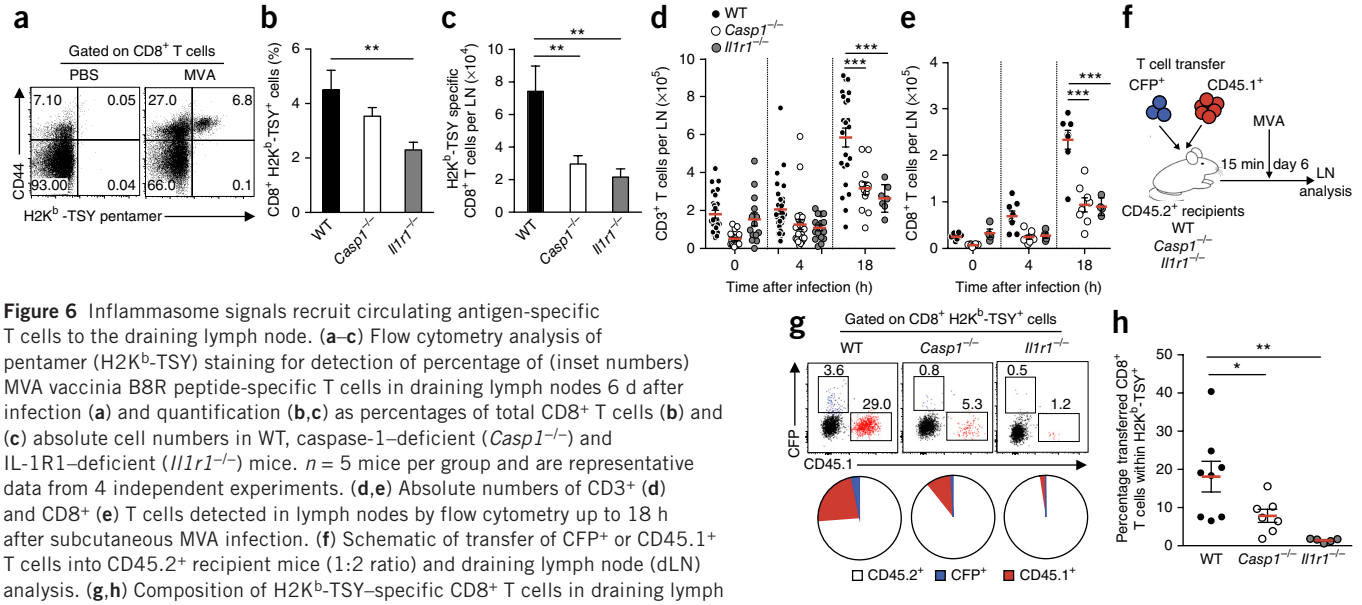

Figure 6 Inflammasome signals recruit circulating antigen-specific T cells to the draining lymph node. (**a**–**c**) Flow cytometry analysis of pentamer (H2K^b-TSY) staining for detection of percentage of (inset numbers) MVA vaccinia B8R peptide-specific T cells in draining lymph nodes 6 d after infection (**a**) and quantification (**b**,**c**) as percentages of total CD8$^+$ T cells (**b**) and (**c**) absolute cell numbers in WT, caspase-1–deficient (*Casp1*$^{-/-}$) and IL-1R1–deficient (*Il1r1*$^{-/-}$) mice. $n = 5$ mice per group and are representative data from 4 independent experiments. (**d**,**e**) Absolute numbers of CD3$^+$ (**d**) and CD8$^+$ (**e**) T cells detected in lymph nodes by flow cytometry up to 18 h after subcutaneous MVA infection. (**f**) Schematic of transfer of CFP$^+$ or CD45.1$^+$ T cells into CD45.2$^+$ recipient mice (1:2 ratio) and draining lymph node (dLN) analysis. (**g**,**h**) Composition of H2K^b-TSY–specific CD8$^+$ T cells in draining lymph nodes 6 d after MVA infection showing transferred CFP$^+$ (blue) and CD45.1$^+$ (red) T cells. Inset numbers indicate percentage of population. Percentages as a proportion of total pentamer-specific T cells are represented in the pie charts (**g**, bottom) and summarized in **h**. Combined data from three independent experiments (n = more than 7 mice per group). Error bars, mean ± s.e.m. $^*P < 0.05$, $^{**}P < 0.01$, $^{***}P < 0.001$, one-way ANOVA with Tukey's multiple comparison test.

immediately administered local MVA infection (**Fig. 6f**) so that the majority of transferred T cells were present in the circulation at the time of infection. We transferred a combination of T cells that could be subsequently re-traced *in vivo*, each at a different ratio to provide minor circulating T cell populations and simulate an *in vivo* limiting-dilution assay. We analyzed the specific contribution of transferred T cells in the bulk of the VVp-specific T cell pool at the peak of the response to evaluate the mobilization of T cells that were not initially present in the lymph node. In WT mice, a large fraction of the VVp response was derived from the transferred T cell populations. However, this contribution was reduced in caspase-1–deficient and even more so in IL-1R1–deficient mice (**Fig. 6g**,**h**). In particular, the CFP$^+$ T cells (which were transferred in the lowest numbers) were virtually absent from the VVp-specific response in caspase-1– and IL-1R1–deficient mice. We confirmed that this effect was attributed to the defective early recruitment of adoptively transferred T cells from the circulation to infection-draining lymph nodes in the absence of inflammasome signaling (**Supplementary Fig. 6**). As expected, delaying MVA injection until 48 h after T cell transfer to allow time for transferred T cells to equilibrate within lymphoid organs resulted in an overall T cell response that was less dependent on early inflammasome-driven T cell recruitment, with transferred T cells making similar contributions toward the overall VVp-specific T cell response in WT mice and mice with disrupted inflammasome signaling (**Supplementary Fig. 6b**).

In line with these findings, blocking T cell trafficking to the draining lymph node during MVA infection in WT mice using a CD62L-specific blocking antibody resulted in a significant reduction in the number of VVp-specific T cells (**Supplementary Fig. 7a**,**b**). Furthermore, analysis of IFN-γ T cell responses to other H-2K^b-restricted peptide epitopes for MVA (A3L, K3L, A19L and A8R) showed that blocking T cell recruitment also reduced the diversity of the T cell response (**Supplementary Fig. 7c**,**d**) further highlighting the importance of T cell trafficking to the draining lymph node for optimal responses. These data indicate that inflammasome activation increases the magnitude and broadens the potential repertoire of the T cell response by mobilizing antigen-specific T cell clones from the periphery.

DISCUSSION

Secondary lymphoid organs are key locations for initiation of innate host defense and priming of the adaptive response. Here we provide evidence of a host immune circuit linking activation of these two arms of the response to deliver effective immunity, which is coordinated through inflammasome signaling initiated by subcapsular macrophage sensing of infection.

Methods to detect inflammasome activation *in situ* have so far been very limited, relying primarily on tissue histological staining for speck protein components, active caspase-1 or mature IL-1β[8,39–41]. This task is further complicated by the close link between inflammasome activation and cell death and the inherent difficulty in detecting such transient events[42]. Our approach circumvents these limitations by probing the inflammasome in real-time and in single cells using intravital imaging. A potential caveat of our strategy may be that ASC overexpression alters the timing of inflammasome activation. However, this was not observed *in vitro*, and furthermore, the kinetics of the immune response to MVA and SCS macrophage death in our chimeras was similar to that observed in WT mice, suggesting that overexpression of the probe has no obvious effect on the observed response. With the ability to detect the cell type, location and timing of inflammasome pathway, we provide the first glimpse into the dynamics of inflammasome activation in the context of lymph-borne virus. As recent *in vitro* studies have demonstrated that the kinetics of caspase-1 activation are essentially the same irrespective of the intensity or types of stimulus[4,43], our results may be directly relevant to other types of pathogenic challenges *in vivo*.

A recent study by Kastenmüller *et al.* has indicated a role for the inflammasome pathway in innate immune cell activation and recruitment in response to lymph-borne pathogens, highlighting an important role for SCS macrophages in the context of IL-18 and IL-1β release[16]. In addition, this report and previous work show that SCS

depletion alters neutrophils and NK cell recruitment in the draining lymph node upon viral challenge[16,33]. The present results extend these findings by demonstrating directly that macrophages in the subcapsular area of the lymph node rapidly undergo inflammasome activation, which is immediately followed by pyroptotic cell death. Although our data support the idea that SCS macrophages are the major population undergoing inflammasome activation during the early phase of the response, it is likely that other cell types, such as inflammatory monocytes or neutrophils, may also contribute to the inflammasome response during later stages of infection[44,45]. Our results provide *in vivo* support for the idea that the inflammasome acts as a digital switch, whereby pyroptosis coincides with a burst-release of proinflammatory cytokines, which are rapidly processed by concomitant caspase-1 activation, a phenomenon recently described *in vitro*[42,43]. Thus, *in vivo*, inflammasome signaling by subcapsular sinus macrophages probably delivers a concentrated and localized inflammatory stimulus to surrounding cells, defining a discrete anatomical compartmentalization of the inflammasome response.

Extracellular ASC specks are active when injected *in vivo*[8,9], but their generation *in situ* has not, to our knowledge, been characterized previously. We now directly demonstrate that most ASC specks persist for several hours as extracellular structures before showing signs of degradation. Detection of speck fragmentation and engulfment *in vivo* suggests that these events may provide potential mechanisms of amplifying the inflammasome response and warrant further examination of the functional relevance of these phenomena in contributing toward the immune response.

One potential consequence of lymph-borne infection is the alteration of the SCS macrophage layer. Neutrophil or dendritic cell infiltration can contribute to disruption and/or destruction of this layer[46,47]. Our results establish pyroptosis as an additional, direct mechanism accounting for the clearance of $CD169^+$ SCS macrophages observed during infection[47]. Local recruitment of myeloid cells triggered by inflammasome activation and pyroptosis is reminiscent of neutrophil clustering observed around dying cells[46,48,49]. Although this immediate response is probably due to the release of local mediators upon cell death, such as extracellular ATP or other DAMPs[50–52], our results suggest that subsequent IL-1 sensing by hematopoietic cells largely amplifies the initial inflammasome signals. This second level of signal propagation resulting in chemokine production and cellular recruitment to the draining lymph node may therefore work in concert with other mechanisms of lymph node remodeling induced by infection, such as vascular and lymph angiogenesis leading to increased organ volume[53].

Emerging data are highlighting the importance of inflammasome regulation of the adaptive T cell response in the context of vaccine adjuvanticity, infection and autoimmune disorders[54–58]. In several studies, lack of inflammasome activity has been shown to result in a poorer T cell response to infection[19,57,58]. Triggering of the inflammasome pathway may increase the quality of antigen presentation or act on T cell differentiation and expansion through the direct action of IL-1 (refs. 24,59). Here we have uncovered an additional mechanism whereby inflammasome activation enhances the magnitude and breadth of composition of T cell responses by promoting recruitment of T cells from the periphery. MVA and other vaccine vectors that engage the inflammasome pathway may therefore be advantageous in mobilization of a maximal number of antigen-specific T cell clones to the draining lymph node.

In summary, our results reveal an immune circuit operating in lymph nodes in which a spatially compartmentalized wave of inflammasome activation translates into the massive recruitment of innate and adaptive immune cells that ultimately maximizes T cell responses. Our approach to probing inflammasome activity *in vivo* will allow dissecting the contribution of this pathway in vaccination, infection or inflammatory disease.

METHODS

Methods and any associated references are available in the online version of the paper.

Note: Any Supplementary Information and Source Data files are available in the online version of the paper.

ACKNOWLEDGMENTS

We wish to thank O. Schwartz, N. Manel and members of P.B.'s laboratory for critical review of the manuscript; A. Cumano (Institut Pasteur) for helpful discussions in generating BM chimeric mice; and the Centre d'Immunologie Humaine (Institut Pasteur) for support with flow cytometry. This work was supported by Institut Pasteur (P.B.), Institut National de la Santé et de la Recherche Médicale (P.B.), the Vaccine Research Institute (P.B.), Fondation pour la Recherche Médicale (P.B.) and a Starting Grant from the European Research Council (P.B.).

AUTHOR CONTRIBUTIONS

P.B. and P.S. designed the experiments, analyzed the data and wrote the manuscript; P.S. and B.B. conducted the experiments with essential support from Z.G., F.L.; D.M., M.L.A. and Y.L. provided scientific input and reagents.

COMPETING FINANCIAL INTERESTS

The authors declare no competing financial interests.

1. Monie, T.P., Moncrieffe, M.C. & Gay, N.J. Structure and regulation of cytoplasmic adapter proteins involved in innate immune signaling. *Immunol. Rev.* **227**, 161–175 (2009).
2. Franchi, L., Muñoz-Planillo, R. & Núñez, G. Sensing and reacting to microbes through the inflammasomes. *Nat. Immunol.* **13**, 325–332 (2012).
3. Bryan, N.B., Dorfleutner, A., Rojanasakul, Y. & Stehlik, C. Activation of inflammasomes requires intracellular redistribution of the apoptotic speck-like protein containing a caspase recruitment domain. *J. Immunol.* **182**, 3173–3182 (2009).
4. Lu, A. *et al.* Unified polymerization mechanism for the assembly of ASC-dependent inflammasomes. *Cell* **156**, 1193–1206 (2014).
5. Fernandes-Alnemri, T. *et al.* The pyroptosome: a supramolecular assembly of ASC dimers mediating inflammatory cell death via caspase-1 activation. *Cell Death Differ.* **14**, 1590–1604 (2007).
6. Stutz, A., Horvath, G.L., Monks, B.G. & Latz, E. ASC speck formation as a readout for inflammasome activation. *Methods Mol. Biol.* **1040**, 91–101 (2013).
7. Mariathasan, S. *et al.* Differential activation of the inflammasome by caspase-1 adaptors ASC and Ipaf. *Nature* **430**, 213–218 (2004).
8. Franklin, B.S. *et al.* The adaptor ASC has extracellular and 'prionoid' activities that propagate inflammation. *Nat. Immunol.* **15**, 727–737 (2014).
9. Baroja-Mazo, A. *et al.* The NLRP3 inflammasome is released as a particulate danger signal that amplifies the inflammatory response. *Nat. Immunol.* **15**, 738–748 (2014).
10. Compan, V. *et al.* A genetically encoded IL-1β bioluminescence resonance energy transfer sensor to monitor inflammasome activity. *J. Immunol.* **189**, 2131–2137 (2012).
11. Compan, V. *et al.* Cell volume regulation modulates NLRP3 inflammasome activation. *Immunity* **37**, 487–500 (2012).
12. Kindermann, M. *et al.* Selective and sensitive monitoring of caspase-1 activity by a novel bioluminescent activity-based probe. *Chem. Biol.* **17**, 999–1007 (2010).
13. Bartok, E. *et al.* iGLuc: a luciferase-based inflammasome and protease activity reporter. *Nat. Methods* **10**, 147–154 (2013).
14. Dinarello, C.A. Immunological and inflammatory functions of the interleukin-1 family. *Annu. Rev. Immunol.* **27**, 519–550 (2009).
15. Rider, P. *et al.* IL-1α and IL-1β recruit different myeloid cells and promote different stages of sterile inflammation. *J. Immunol.* **187**, 4835–4843 (2011).
16. Kastenmüller, W., Torabi-Parizi, P., Subramanian, N., Lämmermann, T. & Germain, R.N. A spatially-organized multicellular innate immune response in lymph nodes limits systemic pathogen spread. *Cell* **150**, 1235–1248 (2012).
17. Rowe, S.J., Allen, L., Ridger, V.C., Hellewell, P.G. & Whyte, M.K. Caspase-1–deficient mice have delayed neutrophil apoptosis and a prolonged inflammatory response to lipopolysaccharide-induced acute lung injury. *J. Immunol.* **169**, 6401–6407 (2002).
18. Gross, O. *et al.* Syk kinase signalling couples to the Nlrp3 inflammasome for anti-fungal host defence. *Nature* **459**, 433–436 (2009).

19. Ichinohe, T., Lee, H.K., Ogura, Y., Flavell, R. & Iwasaki, A. Inflammasome recognition of influenza virus is essential for adaptive immune responses. *J. Exp. Med.* **206**, 79–87 (2009).
20. Shio, M.T. *et al.* Malarial hemozoin activates the NLRP3 inflammasome through Lyn and Syk kinases. *PLoS Pathog.* **5**, e1000559 (2009).
21. Lima-Junior, D.S. *et al.* Inflammasome-derived IL-1β production induces nitric oxide-mediated resistance to Leishmania. *Nat. Med.* **19**, 909–915 (2013).
22. Ghiringhelli, F. *et al.* Activation of the NLRP3 inflammasome in dendritic cells induces IL-1β-dependent adaptive immunity against tumors. *Nat. Med.* **15**, 1170–1178 (2009).
23. Chung, Y. *et al.* Critical regulation of early Th17 cell differentiation by interleukin-1 signaling. *Immunity* **30**, 576–587 (2009).
24. Ben-Sasson, S.Z. *et al.* IL-1 enhances expansion, effector function, tissue localization, and memory response of antigen-specific CD8 T cells. *J. Exp. Med.* **210**, 491–502 (2013).
25. Delaloye, J. *et al.* Innate immune sensing of modified vaccinia virus Ankara (MVA) is mediated by TLR2-TLR6, MDA-5 and the NALP3 inflammasome. *PLoS Pathog.* **5**, e1000480 (2009).
26. Waibler, Z. *et al.* Modified vaccinia virus Ankara induces Toll-like receptor-independent type I interferon responses. *J. Virol.* **81**, 12102–12110 (2007).
27. Hornung, V. *et al.* AIM2 recognizes cytosolic dsDNA and forms a caspase-1-activating inflammasome with ASC. *Nature* **458**, 514–518 (2009).
28. Gross, O., Thomas, C.J., Guarda, G. & Tschopp, J. The inflammasome: an integrated view. *Immunol. Rev.* **243**, 136–151 (2011).
29. Gross, O. Measuring the inflammasome. *Methods Mol. Biol.* **844**, 199–222 (2012).
30. Iwasaki, A. A virological view of innate immune recognition. *Annu. Rev. Microbiol.* **66**, 177–196 (2012).
31. Junt, T. *et al.* Subcapsular sinus macrophages in lymph nodes clear lymph-borne viruses and present them to antiviral B cells. *Nature* **450**, 110–114 (2007).
32. Kastenmüller, W. *et al.* Peripheral prepositioning and local CXCL9 chemokine-mediated guidance orchestrate rapid memory $CD8^+$ T cell responses in the lymph node. *Immunity* **38**, 502–513 (2013).
33. Garcia, Z. *et al.* Subcapsular sinus macrophages promote NK cell accumulation and activation in response to lymph-borne viral particles. *Blood* **120**, 4744–4750 (2012).
34. Balci-Peynircioglu, B. *et al.* Expression of ASC in renal tissues of familial mediterranean fever patients with amyloidosis: postulating a role for ASC in AA type amyloid deposition. *Exp. Biol. Med. (Maywood)* **233**, 1324–1333 (2008).
35. Phan, T.G., Green, J.A., Gray, E.E., Xu, Y. & Cyster, J.G. Immune complex relay by subcapsular sinus macrophages and noncognate B cells drives antibody affinity maturation. *Nat. Immunol.* **10**, 786–793 (2009).
36. Miao, E.A., Rajan, J.V. & Aderem, A. Caspase-1–induced pyroptotic cell death. *Immunol. Rev.* **243**, 206–214 (2011).
37. Fernandes-Alnemri, T. & Alnemri, E.S. Assembly, purification, and assay of the activity of the ASC pyroptosome. *Methods Enzymol.* **442**, 251–270 (2008).
38. Lehmann, M.H. *et al.* Modified vaccinia virus ankara triggers chemotaxis of monocytes and early respiratory immigration of leukocytes by induction of CCL2 expression. *J. Virol.* **83**, 2540–2552 (2009).
39. Dvoriantchikova, G. *et al.* Genetic ablation of Pannexin1 protects retinal neurons from ischemic injury. *PLoS One* **7**, e31991 (2012).
40. Mezzaroma, E. *et al.* The inflammasome promotes adverse cardiac remodeling following acute myocardial infarction in the mouse. *Proc. Natl. Acad. Sci. USA* **108**, 19725–19730 (2011).
41. Tran, H.B. *et al.* Immunolocalization of NLRP3 inflammasome in normal murine airway epithelium and changes following induction of ovalbumin-induced airway inflammation. *J. Allergy (Cairo)* **2012**, 819176 (2012).
42. Shirasaki, Y. *et al.* Real-time single-cell imaging of protein secretion. *Sci. Rep.* **4**, 4736 (2014).
43. Liu, T. *et al.* Single-cell imaging of caspase-1 dynamics reveals an all-or-none inflammasome signaling response. *Cell Rep.* **8**, 974–982 (2014).
44. Cho, J.S. *et al.* Neutrophil-derived IL-1β is sufficient for abscess formation in immunity against *Staphylococcus aureus* in mice. *PLoS Pathog.* **8**, e1003047 (2012).
45. Seo, S.U. *et al.* Distinct commensals induce interleukin-1β via NLRP3 inflammasome in inflammatory monocytes to promote intestinal inflammation in response to injury. *Immunity* **42**, 744–755 (2015).
46. Chtanova, T. *et al.* Dynamics of neutrophil migration in lymph nodes during infection. *Immunity* **29**, 487–496 (2008).
47. Gaya, M. *et al.* Host response. Inflammation-induced disruption of SCS macroph ages impairs B cell responses to secondary infection. *Science* **347**, 667–672 (2015).
48. Lämmermann, T. *et al.* Neutrophil swarms require LTB4 and integrins at sites of cell death *in vivo*. *Nature* **498**, 371–375 (2013).
49. McDonald, B. *et al.* Intravascular danger signals guide neutrophils to sites of sterile inflammation. *Science* **330**, 362–366 (2010).
50. Lotze, M.T. *et al.* The grateful dead: damage-associated molecular pattern molecules and reduction/oxidation regulate immunity. *Immunol. Rev.* **220**, 60–81 (2007).
51. Zhang, Q. *et al.* Circulating mitochondrial DAMPs cause inflammatory responses to injury. *Nature* **464**, 104–107 (2010).
52. Amaral, F.A. *et al.* NLRP3 inflammasome-mediated neutrophil recruitment and hypernociception depend on leukotriene B_4 in a murine model of gout. *Arthritis Rheum.* **64**, 474–484 (2012).
53. Kumar, V. *et al.* Global lymphoid tissue remodeling during a viral infection is orchestrated by a B cell-lymphotoxin-dependent pathway. *Blood* **115**, 4725–4733 (2010).
54. Dostert, C., Ludigs, K. & Guarda, G. Innate and adaptive effects of inflammasomes on T cell responses. *Curr. Opin. Immunol.* **25**, 359–365 (2013).
55. Dixit, V.D. Nlrp3 inflammasome activation in type 2 diabetes: is it clinically relevant? *Diabetes* **62**, 22–24 (2013).
56. Yang, M., Hearnden, C.H., Oleszycka, E. & Lavelle, E.C. NLRP3 inflammasome activation and cytotoxicity induced by particulate adjuvants. *Methods Mol. Biol.* **1040**, 41–63 (2013).
57. O'Donnell, H. *et al.* Toll-like receptor and inflammasome signals converge to amplify the innate bactericidal capacity of T helper 1 cells. *Immunity* **40**, 213–224 (2014).
58. Dunne, A. *et al.* Inflammasome activation by adenylate cyclase toxin directs Th17 responses and protection against *Bordetella pertussis*. *J. Immunol.* **185**, 1711–1719 (2010).
59. Ben-Sasson, S.Z. *et al.* IL-1 acts directly on CD4 T cells to enhance their antigen-driven expansion and differentiation. *Proc. Natl. Acad. Sci. USA* **106**, 7119–7124 (2009).

ONLINE METHODS

Mice. Wild-type (WT) C57Bl/6 mice were purchased from Charles River France. Caspase-1–deficient (*Casp1*$^{-/-}$ *Casp4/11*$^{-/-}$, B6N.129S2-Casp1^{tm1Flv}/J)[60], IL-1R1–deficient (*Il1r1*$^{-/-}$, B6.129S7-Il1r1^{tm1Imx}/J), C57Bl/6 *Rag2*$^{-/-}$, CD45.1^{+} (B6.SJL-Ptprc^{a}Pepc^{b}/BoyJ), C57Bl/6-GFP (expressing GFP under the ubiquitin promoter) and C57Bl/6-CFP (expressing CFP under the actin promoter) mice were bred in the animal facility of Institut Pasteur under specific pathogen–free conditions, and littermates were randomly assigned to experimental treatment groups. Experimental protocols were ethically approved by the Institutional Committees on Animal Welfare at Institut Pasteur and conducted in strict accordance with French guidelines for animal care and use.

Treatments and reagents. Recombinant MVA-B (expressing full-length HIV Gag, fused to three Pol and two Nef fragments)[61] was provided by the Agence Nationale de Recherche sur le Sida (ANRS), and a recombinant MVA-B strain expressing enhanced GFP was provided by Transgene Laboratories (Strasbourg, France). Mice were injected subcutaneously (s.c.) in the footpad with 5×10^6 p.f.u. of MVA. *In vivo* labeling of CD169^{+} cells was performed by s.c. injection of 0.5 µg PE-conjugated anti-CD169 (Biolegend, clone 3D6.112) approximately 1 h before imaging. *In vivo* staining of extracellular ASC specks was performed by injection of 0.5 µg AF555-conjugated anti-ASC antibody (Bioss Antibodies, bs-6741R-A555) 6 h after MVA or PBS injection, and imaging commenced within 30 min. Whole lymph node labeling with Hoechst 33342 (33342 trihydrochloride, trihydrate, Invitrogen) was performed by s.c. injection of 10 µL of a 0.1 µM solution prepared in PBS, and imaging commenced within 30 min. The investigators were not blinded to group allocation during experiments or data analysis. *In vivo* blockade of CD62L was performed by intravenous (i.v.) injection of 100 µg blocking antibody (ebioscience, MEL-14) 6 h before MVA injection and 24 h after MVA injection. WT mice were treated with IL-1β–neutralizing antibody (R&D systems, AF-401-NA) by administration of 100 µg intraperitoneally (i.p.) 1 h before T cell transfer or MVA injection.

Flow cytometry. To detect caspase activity, macrophages (0.2×10^6 cells) were seeded in ultra-low attachment 24-well plates (Corning) overnight and then stimulated with MVA expressing a fluorescent protein to monitor infection at a multiplicity of infection (MOI) of 1, 5, 25 or 50 for 6–10 h. Cells were gently harvested and stained with a FLICA-1 FITC (caspase-1 probe FAM-YVAD-FMK) and FLICA-3/7 660 (caspases-3/7 FAM-DEVD-FMK) kits according to the manufacturer's instructions (Immunochemistry Technologies). Control cultures were treated with 1 µM staurosporine (STS) (Sigma) to induce caspase-3 activity. To detect tissue infection by MVA and inflammatory cell recruitment, popliteal lymph nodes were teased apart using forceps and digested in RPMI 1640 containing 1 mg/ml collagenase D and 50 ng/ml DNase (Sigma) for 15 min at 37 °C, and then passed through a 70-µm cell strainer. Virally expressed GFP was detectable directly by flow cytometry. Cell-surface staining was performed with the following antibodies, all from Biolegend and at a dilution of 1:200 (0.5 µg/mL) unless otherwise specified, in the presence of blocking anti-CD16/32 (eBioscience, clone 93) and after exclusion of doublets and dead cells (live/dead fixable dyes, Invitrogen): anti-CD3 (17A2), anti-NK.1.1 (PK136), anti-CD8 (53-6.7), anti-CD19 (1D3), anti-CD169 (3D6.112/ MOMA-1, AbD Serotec,), anti-CD11b (M1/70, BD), anti-F4/80 (BM8), anti-CD45.1 (A20), anti-CD45.2 (104), anti-CD11c (N418), (1:500) anti-I-A/E (M5/114.15.2), (1:400) anti-Ly-6G (1A8), anti-Ly-6C (AL-21). Cell subset analysis was performed on the basis of the following phenotypic gating definitions: CD3^{-} CD11b^{+} CD169^{+} F4/80^{-} for SCS-M, CD3^{-}CD11b^{+}CD169^{+}F4/80^{+} for Med-M, CD3^{-} Ly6G^{-}CD169^{-}CD11b^{+} for macrophages, CD3^{-}I-A/E^{hi}CD11c^{+} for DCs, CD3^{-} Ly6G^{-}Ly6C^{hi}CD11b^{+} for inflammatory monocytes, CD11b^{hi}Ly6G^{+} for neutrophils and CD11b^{+}NK1.1^{+} for NKs cells. Absolute cell numbers were quantified using AccuCheck bead microspheres (Life Technologies) during flow acquisition. Intracellular staining was performed using the Cytofix/Cytoperm kit (BD Bioscience) using APC-conjugated anti-granzyme B (GB11, BD biosciences) and FITC-conjugated anti-IFNγ (XMG1.2, ebioscience). Analyses were performed using an LSRII Cytometer (BD Biosciences) and analyzed using FlowJo software version 10.6 (Tree Star). Cell death induced by MVA was detected in BMDM cultures infected with MVA-GFP by counterstaining with 2.5 µg/mL propidium iodide (Sigma).

ELISA. For ELISA detection of IL-1β in cell-free supernatants, BMDMs were cultured overnight with MVA (MOI 1–50) or 1 µg/mL LPS (serotype 026:B6, Sigma) in the presence or absence of 75 µM caspase-1 inhibitor Z-YVAD-FMK (R&D Systems). The next day, LPS-treated cells were pulsed with 5 mM ATP for 1 h. Supernatants were harvested and analyzed using IL-1β DuoSet ELISA kit according to the manufacturer's instructions (R&D Systems).

Inflammasome ASC probe generation. ASC-GFP (enhanced GFP) or ASC-mCherry (monomeric cherry)[6] constructs encoding the full sequence of ASC with a fluorescent protein tag on the 5′ sequence end were cloned into a murine stem cell viral (MSCV) vector using standard techniques. Retrovirus was generated by co-transfection of ASC-MSCV (30 µg) and pCI-Eco (10 µg) plasmid DNA into HEK293T cells using Lipofectamine 2000 transfection reagent (60 µL) (Life Technologies) in Opti-MEM (Gibco). Transfection was quenched after 8 h with DMEM containing 10% FBS, 1% penicillin/ streptomycin. After overnight incubation at 37 °C, culture medium was replaced with either complete DMEM or Iscove's Modified Dulbecco's Medium (IMDM) for transduction of BMDMs or hematopoietic stem cells (HSCs), respectively. Retrovirus containing supernatant was harvested from HEK293T cell cultures during the next 2 d, filtered (0.45 µM) and used to perform sequential rounds of BMDM and HSC transduction as described below.

Bone marrow–derived macrophage generation and transduction. Murine bone marrow–derived macrophages (BMDMs) from WT or *Casp1*$^{-/-}$ mice were differentiated from bone marrow ($1–1.5 \times 10^6$ cells seeded in 9.5-cm^2 wells) by culture in DMEM, 10% FBS, 1% penicillin/streptomycin, 1% HEPES (all from Gibco) with 20 ng/mL macrophage-colony stimulating factor (M-CSF, eBioscience) or 20% L929 supernatant, and used at day 7. BMDMs were stably transduced to express ASC-GFP or mCherry by adding retroviral-conditioned medium to macrophage cultures on days 3 and 4 during differentiation. Retroviral supernatant was supplemented with fresh DMEM, 10% FBS, 14 µg/mL polybrene (Sigma), 1% HEPES and 20 ng/mL M-CSF (eBioscience) to prepare retroviral conditioned medium, which was used to replace medium on BMDM cultures and incubated at 37 °C overnight. On day 5, retroviral medium was replaced with fresh culture medium, and cultures were maintained until day 7 for use. Transduction efficiencies of >70% were routinely achieved.

Time-lapse videomicroscopy. Macrophages transduced to express ASC-GFP or ASC-mCherry (0.2×10^6 cells) were seeded in 35-mm FluoroDish cell culture dishes (World Precision Instruments) in phenol red–free RPMI supplemented with 10% FBS, 1% penicillin/streptomycin and 10 ng/mL M-CSF for 6 h, with additional 1 µg/mL LPS where indicated. Immediately before imaging, cell medium was replaced with medium containing MVA, MVA-GFP or 5 mM ATP and supplemented with 0.1 µM SytoxBlue (Invitrogen). Time-lapse microscopy was performed using a DMI6000B inverted microscope (Leica Microsystems) equipped with heated chamber for temperature, humidity, and CO_2 control, with a 10×/0.75 NA dry objective (Olympus) and a CoolSNAP HQ2 Roper camera (Photometrics) for 15 h after induction. Videos were analyzed using ImageJ or FiJi softwares (http://rsb.info.nih.gov/ij/).

Bone marrow chimeras. To generate mixed BM chimeric mice for intravital imaging of inflammasome activity, lethally irradiated mice were reconstituted with BM-derived HSCs retrovirally transduced to stably express ASC-GFP protein. Donor HSCs used for reconstitution were negatively selected (Miltenyi Lineage Cell Depletion Kit) from C57Bl/6 *Rag*$^{-/-}$ BM (to achieve myeloid-restricted probe expression) and cultured overnight ($2–3 \times 10^6$ cells per 9.5-cm^2 well) in complete IMDM supplemented with 10% FBS, 1% HEPES, 0.1% 2-mercaptoethanol, 20 ng/mL stem cell factor/c-Kit ligand (SCF) and 10 ng/mL thrombopoietin (TPO). After culture overnight, HSC cultures were resuspended in ASC-GFP retroviral supernatant (supplemented with 10% FBS, 1% HEPES, 0.1% 2-mercaptoethanol, 20 ng/mL SCF, 10 ng/mL TPO, 10 µg/mL polybrene) and spin-transduced at 1,000 × *g* and 32 °C for 90 min. Fresh complete IMDM was added after a further 4–6-h incubation at 37 °C. This was repeated the following day, with the exception that 4–6 h after spin-transduction, HSCs were harvested, washed in fresh medium, and seeded onto pre-prepared 10-cm^2 dishes of OP-9 feeder cells (ATCC)[62] in complete IMDM. Cultures

doi:10.1038/nm.4016

were harvested after a further 36–48 h, and ASC-GFP$^+$ cells sorted on a FACSAria II (Becton Dickenson). Recipient WT mice were lethally irradiated by X-ray (8.5 Gy, X-Xstrahl RS320) 4–6 h before injection of >0.2 × 10^6ASC-GFP HSCs per mouse. Sorted ASC-GFP$^+$ HSCs were injected in combination with either WT or *Casp1*$^{-/-}$ BM HSCs to achieve 90–10% chimerism. This served to restrict caspase-1 functional inflammasome signaling only to probe-expressing cells when used for experiments to examine inflammasome effector functions and also enabled a discrete distribution of ASC-GFP$^+$ cells for easier single cell tracking *in vivo*. Chimeric mice had a normal lymphoid architecture, as mixed chimeras were generated partially with replete BM to reconstitute the lymphoid compartment. Recipient mice were administered sulfamethoxazole and trimethoprim supplemented water (Roche) for the following 2 weeks and were used >8 weeks following BM reconstitution, which was verified by histological and flow cytometry examination of blood and lymphoid tissues. Bone marrow–chimeric mice to study IL-1 sensing were prepared by transferring freshly isolated bone marrow cells (50–100 × 10^6 cells) derived from CD45.1$^+$ *Il1r1*$^{-/-}$ mice into lethally irradiated CD45.2$^+$ WT recipients. Reconstitution of typically >95% was confirmed by blood and lymphoid tissue congenic marker expression.

Whole-tissue chemokine profiling. Multianalyte profiling of whole popliteal lymph node tissue homogenates was done by RodentMAP analysis (MyriadRBM). Popliteal lymph node specimens were prepared 4 h after MVA or PBS injection by pooling 4 excised lymph nodes and homogenizing tissues using a Potter-Elvehjem homogenizer in 350 µl of lysis buffer (50 mM Tris-HCL, pH 7.4, 2 mM EDTA) containing aprotinin, antipain, leupeptin, and pepstatin A (all at 1 µg/mL) and 2 mM PMSF, at 4 °C (Roche Diagnostics). Total protein content of each tissue lysate was quantified (BCA Assay, Pierce) and used to normalize concentrations of analytes detected within each sample to the total sample protein content.

Immunofluorescence histological analysis. Whole excised lymph nodes were fixed at 4 °C overnight in paraformaldehyde and progressively dehydrated in sucrose. Tissues were snap frozen in OCT compound (Tissue-Tek; Sakura) and 8-µm thick tissue cryosections prepared. Antibody staining of F4/80, CD169 and GFP (Invitrogen, PA1-46326) was performed after blocking in mouse and rat serum, and sections were imaged using a confocal microscope (Olympus BX61WI).

Intravital two-photon imaging. Two-photon imaging of intact popliteal lymph node was performed as previously described[33,63] using an upright microscope (DM6000B, Leica Microsystems) with a 20×/0.95 NA water-dipping objective (Olympus). Excitation was provided by a Chameleon Ultra Ti:Sapphire (Coherent) tuned to 950 nm. The following filter sets were used for imaging second harmonics generation (SHG)/GFP/PE and Hoechst/GFP: 483/32 BP, 495 LP, 520/35 BP, 562 LP, 607/20 B; 483/32 BP, 495 LP, 520/35 BP. Image fields of 1,024 × 1,024 pixels, with a mean pixel size of 0.5 µm, *z*-spacing of 4 µm and a volume depth of up to 100 µm were recorded. Data sets were processed and analyzed using Imaris (Bitplane) and FiJi software.

Antigen-specific T cell detection. Antigen-specific T cell responses induced by MVA were detected within spleen and draining popliteal lymph nodes 6 d after infection using contralateral PBS-treated lymph nodes as controls. CD8$^+$ T cells with specificity for the immunodominant vaccinia viral peptide (VVp) B8R 20–27 were detected by pentamer staining (PE-conjugated H2-K^b-TSYKFESV, Proimmune) of whole lymphoid cell suspensions, in CD8$^+$ CD19$^-$ and NK1.1$^-$ gated cells by flow cytometry. For adoptive transfer assays to assess recruitment and antigen-specific T cell priming of peripherally recruited T cells, we purified CD3$^+$ T cells from C57Bl/6-GFP (20 × 10^6 cells), or C57Bl/6-CFP and CD45.1$^+$ mice (10 × 10^6 and 20 × 10^6 cells, respectively) and injected cells 10 × 10^6 and 20 × 10^6 cells, respectively, into CD45.2$^+$ WT, *Casp1*$^{-/-}$ and *Il1r1*$^{-/-}$ mice, followed by s.c. injection of MVA. Six days later, draining lymph node cell suspensions were analyzed by flow cytometry to detect the proportion of transferred cells within pentamer$^+$CD8$^+$CD19$^-$ and NK1.1$^-$ populations. To examine the H2-K^b restricted antigen-specific CD8$^+$ T cell response to MVA peptide antigens A8R (189, ITYRFYLI), A3L (270-277, KSYNYMLL), B8R (20-27, TSYKFESV), K3L (6-15, YSLPNAGDVI), and A19L (47-55, VSLDYINTM) (Polypeptide Laboratories), 1 × 10^6 cells isolated from draining lymph nodes 6 d after MVA injection were cultured in the presence or absence of 1 µg/mL of each peptide and 1× GolgiPlug (BD bioscience) in complete medium for 4 h, followed by intracellular cytokine staining.

Statistical analyses. All statistical tests were performed using GraphPad Prism 6.0b, and all data are represented as mean ± s.e.m. Group comparisons were assessed with nonparametric tests. We used Student's *t*-test to compare two groups and Kruskal-Wallis test for multiple comparisons.

One-way ANOVA test followed by Tukey's *post hoc* test was used for multiple comparisons of data with normal distribution and equal variance. All statistical tests were two-tailed, and significance was defined as $P < 0.05$. $^*P < 0.05$, $^{**}P < 0.01$, $^{***}P < 0.001$. No statistical test was used to predetermine sample size, and all samples were included in the analysis.

60. Kuida, K. *et al.* Altered cytokine export and apoptosis in mice deficient in interleukin-1β–converting enzyme. *Science* **267**, 2000–2003 (1995).
61. Brandler, S. *et al.* Preclinical studies of a modified vaccinia virus Ankara-based HIV candidate vaccine: antigen presentation and antiviral effect. *J. Virol.* **84**, 5314–5328 (2010).
62. Nakano, T., Kodama, H. & Honjo, T. Generation of lymphohematopoietic cells from embryonic stem cell in culture. *Science* **265**, 1098–1101 (1994).
63. Celli, S., Breart, B. & Bousso, P. Intravital two-photon imaging of natural killer cells and dendritic cells in lymph nodes. *Methods Mol. Biol.* **415**, 119–126 (2008).